THE JOURNAL OF PHYSICAL CHEMISTRY B

Article

pubs.acs.org/JPCB

# Pseudo-Rephasing and Pseudo-Free-Induction-Decay Mechanism in Two-Color Three-Pulse Photon Echo of a Binary System

Hui Dong, Ian Seungwan Ryu, and Graham R. Fleming*

Department of Chemistry, University of California, Berkeley, California 94720, United States

Physical Biosciences Division, Lawrence Berkeley National Laboratory, Berkeley, California 94720, United States

**ABSTRACT:** We investigate the two-color three-pulse photon echo peak shift in a (left−right) binary system, where each component consists of a heterodimer. On the basis of the model, we find that the effect of the excitonic asymmetry between two components leads to an additional factor in the peak shift. A pseudo-rephasing and pseudo-free-induction-decay mechanism is proposed to explain the resultant negative peak shift, when the differences between the two left/right components have the opposite sign. In such a case, estimates of the electronic coupling strength via two- and one-color peak shift experiments lead to an underestimate of the coupling magnitude.

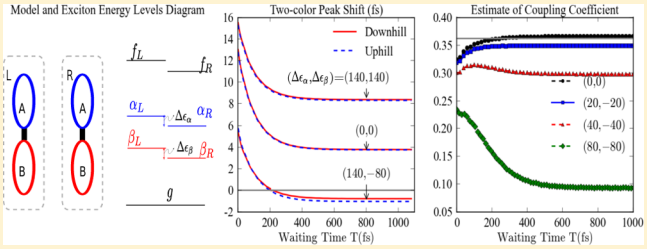


## 1. INTRODUCTION

The three-pulse photon echo peak shift measurements have proved valuable in the study of the solvent and solvation dynamics, which, in turn, play important roles in many chemical and physical processes in the condensed phase.[1,2] In particular, the one-color three-pulse photon echo peak shift measurement was proposed theoretically[3,4] and used experimentally[5−7] to understand the dynamics of solution fluctuation as a direct display of the behavior of the transition frequency correlation function $M(t) = \langle \Delta\omega(t)\Delta\omega(0)\rangle/\langle \Delta\omega\rangle^2$. The photon echo peak shift measurement, being homodyne detected, provides an experimentally simple route to four-wave mixing experiments involving multiple, non-overlapping spectra for the three input pulses. In the system with electronic coupling and dynamics such as energy transfer, the development of the two-color three-pulse photon echo peak shift experiment enabled the measurement of the electronic coupling between chromophores, when used in combination with the one-color three-pulse photon echo peak shift.[8−13]

In these four-wave mixing measurements, three pulses are sent into a sample along different directions, which allows isolation of the photon echo signal via phase matching. In the photon echo direction, the result of the following sequence of events is detected: the first pulse creates a coherence that evolves for time $\tau$, the second pulse creates a population state that evolves for time $T$, and the third pulse creates a second coherence that cancels the phase accumulated during time $\tau$. Physically, the appearance of a finite peak shift value is due to the competition between the rephasing and the loss of rephasing ability as a result of the dynamical process under study. Typically, a non-negative peak shift is expected in these experiments.[3,4] However, recent two-color three-pulse photon echo experiments have reported a negative peak shift on bacterial reaction center[14,15] for small waiting time.[12,13] The negative peak shift was previously interpreted as evidence for a negative correlated transition frequency[3] or as a result of rapid depletion of excitonic population.[12,13] In this paper, we propose an alternative mechanism based on pseudo-rephasing and pseudo-free-induction-decay (FID) in a binary system and understand the negative peak shift as the result of macroscopic interference.[1,16] We evaluate the effect of the electronic energy gap and electronic coupling constant asymmetry between the two components of the binary system.[17−21] A specific example of such a system is the photosynthetic reaction center, which in all known cases possesses an approximate $C_2$ symmetry.

## 2. MODEL

The current paper focuses on the two-color three-pulse photon echo peak shift measurements on a two-component system, where each component consists of a dimer. The structure of the system is illustrated in Figure 1a. We denote the two chromophores on each component as $A$ and $B$, with subscripts, L (left) and R (right). The dimers on two components are chemically identical, but their local environments modify the vertical transition energies and the coupling constants between chromophores. We assume no coupling between the left and right components, since they are spatially well separated from each other.

To illustrate the system clearly, we first introduce the Hamiltonian of one component—the dimer of two coupled chromophores $A$ and $B$:

$$H = H_A + H_B + J|A\rangle\langle B| + J|B\rangle\langle A| \quad (1)$$

**Received:** September 18, 2013
**Revised:** November 15, 2013
**Published:** November 27, 2013

   dx.doi.org/10.1021/jp409352z | J. Phys. Chem. B 2013, 117, 16416−16421

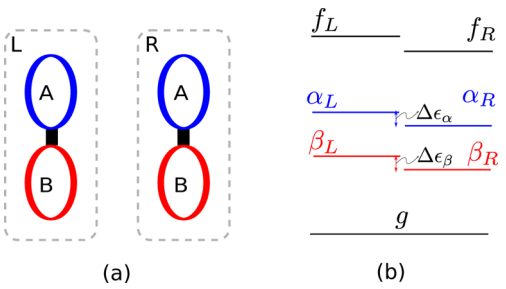


**Figure 1.** Setup of the system. (a) The binary system with each component as a heterodimer. The two chromophores are marked as *A* and *B*. They are coupled with coupling strength *J*. The indices of components are marked as L and R. Here, we assume no coupling between the chromophores on different components. (b) Exciton (denoted by $\alpha$ and $\beta$ for the single excitation states) energy level diagram. The higher exciton level is shown in blue. Due to the asymmetries between the two components (both in the coupling constants and electronic energy levels), the exciton energy levels are slightly different, and denoted as $\Delta\varepsilon_\alpha \equiv \varepsilon_\alpha^L - \varepsilon_\alpha^R$ and $\Delta\varepsilon_\beta \equiv \varepsilon_\beta^L - \varepsilon_\beta^R$.

where $H_A = \varepsilon_A + \sum_\xi \hbar\omega_\xi^A(a_\xi^\dagger a_\xi + 1/2) + |A\rangle\langle A|\hbar\sum_\xi d_\xi^A\omega_\xi^A(a_\xi^\dagger + a_\xi)$ and $H_B = \varepsilon_B + \sum_\xi \hbar\omega_\xi^B(b_\xi^\dagger b_\xi + 1/2) + |B\rangle\langle B|\hbar\sum_\xi d_\xi^B\omega_\xi^B(b_\xi^\dagger + b_\xi)$ are the corresponding Hamiltonians of chromophores *A* and *B*. Here, we neglect the L and R indices of the components. The electronic degrees of freedom are diagonalized with the following transformations

$$|\alpha\rangle = \cos\theta|A\rangle + \sin\theta|B\rangle \tag{2}$$

$$|\beta\rangle = \sin\theta|A\rangle - \cos\theta|B\rangle \tag{3}$$

where $\theta = 1/2\arctan[2J/(\varepsilon_A - \varepsilon_B)]$ is the mixing angle. The corresponding exciton energies read $\varepsilon_\alpha = (\varepsilon_A + \varepsilon_B + ((\varepsilon_A - \varepsilon_B)^2 + 4J^2)^{1/2})/2$ and $\varepsilon_\beta = (\varepsilon_A + \varepsilon_B - ((\varepsilon_A - \varepsilon_B)^2 + 4J^2)^{1/2})/2$. These exciton energy levels are illustrated in Figure 1b. The differences between the corresponding levels are marked as $\Delta\varepsilon_\alpha \equiv \varepsilon_\alpha^L - \varepsilon_\alpha^R$ and $\Delta\varepsilon_\beta \equiv \varepsilon_\beta^L - \varepsilon_\beta^R$ and are explicitly noted in the figure. In the exciton basis, the Hamiltonian is rewritten as

$$\begin{aligned} H = {} & (\varepsilon_\alpha + q_\alpha)|\alpha\rangle\langle\alpha| + (\varepsilon_\beta + q_\beta)|\beta\rangle\langle\beta| \\ & + \sum_\xi \hbar\omega_\xi^B(b_\xi^\dagger b_\xi + 1/2) + \sum_\xi \hbar\omega_\xi^A(a_\xi^\dagger a_\xi + 1/2) \\ & + q_{\alpha\beta}|\alpha\rangle\langle\beta| + \text{h.c.} \end{aligned} \tag{4}$$

where $q_\alpha = \hbar\sum_\xi d_\xi^A\omega_\xi^A(a_\xi^\dagger + a_\xi)\cos^2\theta + \hbar\sum_\xi d_\xi^B\omega_\xi^B(b_\xi^\dagger + b_\xi)\sin^2\theta$ and $q_\beta = \hbar\sum_\xi d_\xi^A\omega_\xi^A(a_\xi^\dagger + a_\xi)\sin^2\theta + \hbar\sum_\xi d_\xi^B\omega_\xi^B(b_\xi^\dagger + b_\xi)\cos^2\theta$ characterize the coupling of excitons $\alpha$ and $\beta$ to their environments. Also, $q_{\alpha\beta}|\alpha\rangle\langle\beta| = [\hbar\sum_\xi d_\xi^A\omega_\xi^A(a_\xi^\dagger + a_\xi) - \hbar\sum_\xi d_\xi^B\omega_\xi^B(b_\xi^\dagger + b_\xi)]\sin\theta\cos\theta|\alpha\rangle\langle\beta|$ describes the excitonic transition between the two excitonic states $|\alpha\rangle$ and $|\beta\rangle$.

The term with $q_{\alpha\beta}$ was neglected in previous theoretical studies.[8,10,22] The reason is as follows: physically, the system, considered here, has a large energy gap between the one-exciton states, in comparison to the reorganization energy. Therefore, it is expected that the exciton transfer rate will be much smaller than the dephasing rate. The traditional peak shift experiments measure the rephasing capability of a dephased coherent state. In this sense, the excitonic population transfer in the measurement window will not make a significant change to the peak shift value.[8] Thus, we also neglect this term in the current discussion. However, such a term may give rise to different phenomena, when resonance exists between the initial state and a discrete vibrational level of the final state.[23] This effect will be discussed in a future study. Theoretically, such an effect can be evaluated by phenomenologically including the energy transfer as an incoherent hopping[24] between chromophores or using a time-nonlocal quantum master equation.[13,25]

## 3. TWO-COLOR THREE-PULSE PHOTON ECHO

In the two-color three-pulse photon echo experiments, there are multiple choices for pulse sequence. In a downhill

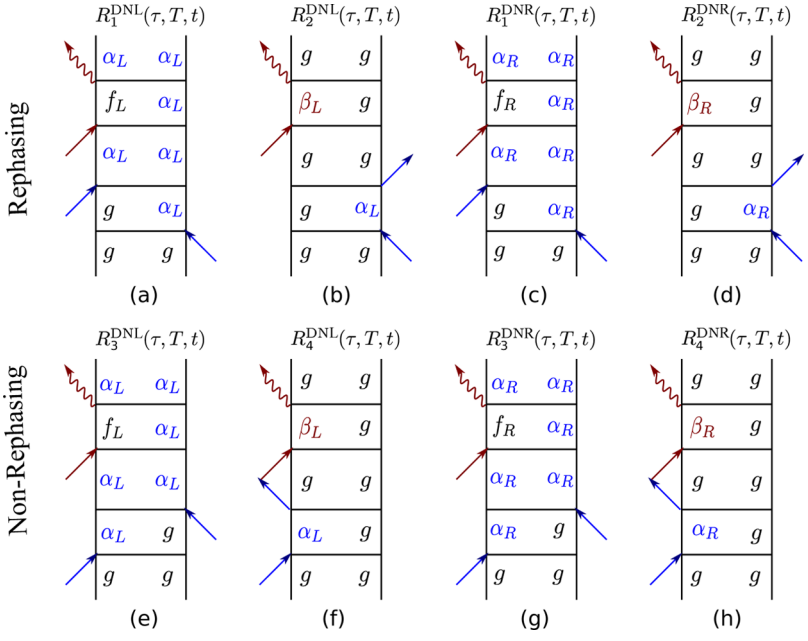


**Figure 2.** The rephasing and non-rephasing pathways in a downhill two-color peak shift experiment on the binary system. (a–d) The rephasing pathways of the left and right components. (e–h) The non-rephasing pathways of the left and right components. The blue (red) color indicates high (low) frequency of the pulse.


dx.doi.org/10.1021/jp409352z | J. Phys. Chem. B 2013, 117, 16416–16421

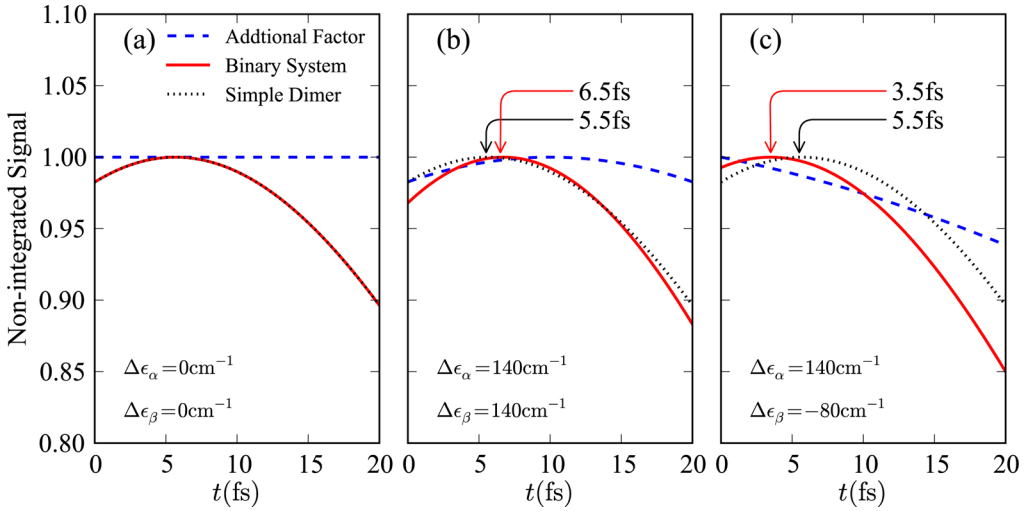


**Figure 3.** The additional factor $\mathcal{A}(\tau, T, t)$ (blue dashed line), the overall signal $|\mathcal{I}^{DN}(\tau, T, t)|^2\mathcal{A}(\tau, t)$ of the binary system shown in Figure 1 (red solid line), and the non-integrated signal $|\mathcal{I}(\tau, T, t)|^2$ (black dotted line) of the single dimer system for the following sets of parameters $\Delta\varepsilon_\alpha$ and $\Delta\varepsilon_\beta$ at temperature $T_e$ = 180 K: (a) $\Delta\varepsilon_\alpha = \Delta\varepsilon_\beta = 0$; (b) $\Delta\varepsilon_\alpha$ = 140 cm$^{-1}$ and $\Delta\varepsilon_\beta$ = 140 cm$^{-1}$; (c) $\Delta\varepsilon_\alpha$ = 140 cm$^{-1}$ and $\Delta\varepsilon_\beta$ = −80 cm$^{-1}$. In the simulation, we choose different Drude−Lorentian spectral densities for chromophores $A$ and $B$, with reorganization energies $\lambda_A$ = 60 cm$^{-1}$ and $\lambda_B$ = 80 cm$^{-1}$ and cutoff frequencies $\omega_{cA} = \omega_{cB}$ = 50 cm$^{-1}$. The inhomogeneous broadenings are $\sigma_A$ = 100 cm$^{-1}$ and $\sigma_B$ = 50 cm$^{-1}$ for chromophores $A$ and $B$, respectively. The mean absorption frequencies of chromophores $A$ and $B$ are adjusted to $\varepsilon_\alpha^0$ = 760 nm and $\varepsilon_\beta^0$ = 800 nm. The mixing angle $\theta$ is set by using a coupling constant $J_0$ = 280 cm$^{-1}$.

measurement, the initial two pulses are higher in energy. The photon echo signal is selected by using phase matching in the direction $\mathbf{k}_s = -\mathbf{k}_1 + \mathbf{k}_2 + \mathbf{k}_3$, where $\mathbf{k}_i$ $(i = 1, 2, 3)$ is the corresponding incident direction of the $i$th pulse. In this signal direction, the first pulse creates a coherence between the high-lying energy level ($|\alpha\rangle$) and the ground state ($|g\rangle$), while the second pulse brings the coherence into a population state. The probe and detection pulse frequencies are at lower frequencies than the first and second pulses, which means the low-lying level ($|\beta\rangle$) is detected. The corresponding responses of the system are illustrated by the double-side Feynman diagrams in Figure 2. Parts a and b show the responses from the left component, while parts c and d illustrate that from the right component. To focus on the mechanism, we assume the impulsive limit[1] in the following discussion. The integrated signal intensity of a single dimer on one component reads

$$I(\tau, t) \propto \int |\mathcal{I}^{DN}(\tau, T, t)|^2 \, dt \tag{5}$$

where $\mathcal{I}^{DN}(\tau, T, t) \equiv R_1^{DN}(\tau, T, t) - R_2^{DN}(\tau, T, t)$ is the non-integrated photon echo signal field of the single dimer with $R_i^{DN}(\tau, T, t)$ $(i = 1, 2)$ as the response functions for the pathways shown in Figure 2a,b. Here, we also neglect the indices of the components. The two response functions are explicitly expressed as

$$\begin{aligned} R_1^{DN}(\tau, T, t) \propto \exp[&i\varepsilon_\alpha\tau - i\varepsilon_\beta t - g_{\alpha\alpha}^*(\tau) + g_{\alpha\beta}(T) \\ &- g_{\beta\beta}(t) - g_{\alpha\beta}^*(\tau + T) - g_{\alpha\beta}(T + t) \\ &+ g_{\alpha\beta}^*(\tau + T + t)] \end{aligned} \tag{6}$$

$$\begin{aligned} R_2^{DN}(\tau, T, t) \propto \exp[&i\varepsilon_\alpha\tau - i\varepsilon_\beta t - g_{\alpha\alpha}^*(\tau) + g_{\alpha\beta}^*(T) \\ &- g_{\beta\beta}(t) - g_{\alpha\beta}^*(\tau + T) - g_{\alpha\beta}^*(T + t) \\ &+ g_{\alpha\beta}^*(\tau + T + t)] \end{aligned} \tag{7}$$

where $g_{\alpha\beta} \equiv (g_A + g_B)\sin^2\theta\cos^2\theta$, $g_{\alpha\alpha} = g_A\cos^4\theta + g_B\sin^4\theta$, and $g_{\beta\beta} = g_A\sin^4\theta + g_B\cos^4\theta$ are the three composite line broadening functions with

$$\begin{aligned} g_i(t) = -\frac{(\sigma_i t)^2}{2} + \frac{2}{\pi}\int d\omega \frac{\mathcal{J}_i(\omega)}{\omega^2}[&(1 - \cos\omega t) \\ &\coth[\beta_e\omega/2] + i(\sin\omega t - \omega t)] \end{aligned} \tag{8}$$

Here, $\mathcal{J}_i(w)$ $(i = A, B)$ is the spectral density of chromophore $i$ and $\sigma_i$ is the corresponding inhomogeneous broadening. We remark here the inhomogeneous broadenings are independently assigned on the sites.[8]

For a heterodyne detection, e.g., 2D electronic spectroscopy,[26,27] the phase factor terms $\exp[i\varepsilon_\alpha\tau - i\varepsilon_\beta t]$ are utilized to locate the positions of the peaks. Since the peak shift measurement generally involves a homodyne detection,[3,22] such a term does not have any influence over the signal of the single dimer and therefore was ignored in previous investigations. However, in our binary system, the asymmetries between components result in different phase factors, which results in macroscopic interference[1,16] of the signals from the two components. On this basis, the overall signal of the binary system follows as

$$I_{Bi}(\tau, t) \propto \int |\mathcal{I}_L^{DN}(\tau, T, t) + \mathcal{I}_R^{DN}(\tau, T, t)|^2 \, dt \tag{9}$$

where $\mathcal{I}_L^{DN}(\tau, T, t)$ and $\mathcal{I}_R^{DN}(\tau, T, t)$ are the corresponding non-integrated signals of left and right components. In the case of identical components, the inhomogeneous broadening is described by a single Gaussian function, which is the same as that of a single dimer. However, the asymmetry between components results in an essentially different inhomogeneous broadening for the same type of chromphore (type A or type B), characterized by the sum of two Gaussian functions, which is not equivalent to that of the single dimer.

To simplify the discussion, we assume that the coupling constants $J$ and the electronic energy gaps $\Delta = \varepsilon_A - \varepsilon_B$ are


dx.doi.org/10.1021/jp409352z | J. Phys. Chem. B 2013, 117, 16416−16421

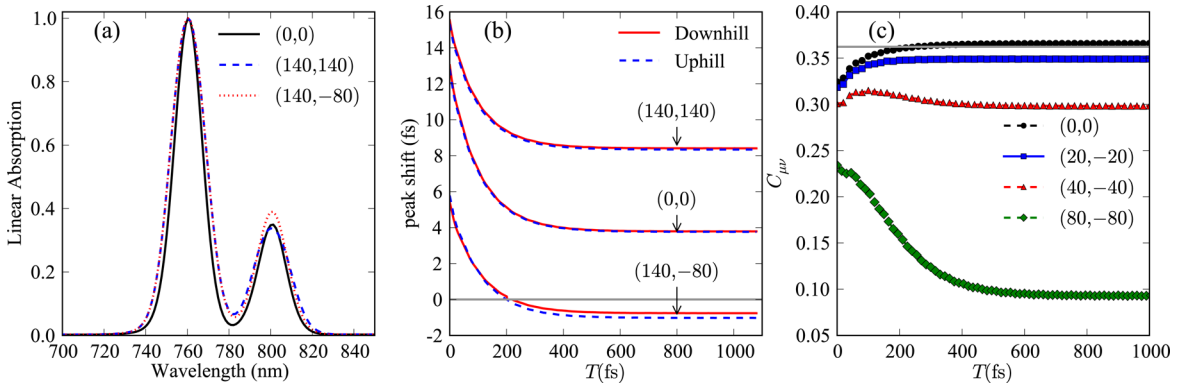


**Figure 4.** Linear absorption spectra, two-color three-pulse peak shift, and coupling coefficient $C_{\mu\nu}$ (see text). (a) Linear absorption spectrum with three parameter sets: (1) $(\Delta\varepsilon_\alpha, \Delta\varepsilon_\beta) = (0, 0)$ (solid line); (2) (140 cm$^{-1}$, 140 cm$^{-1}$) (blue dashed line); (3) (140 cm$^{-1}$, −80 cm$^{-1}$) (red dotted line). (b) Peak shift values for both downhill (red solid line) and uphill (blue dashed line) experiments with the three sets of parameters. (c) Estimated coupling coefficient $C_{\mu\nu}$ as a function of population time $T$. The exact value $C_{\mu\nu}$ (0.362) is given by the gray solid line. In the simulation, all the other parameters are the same as those in Figure 3.

different for the two components, while the mixing angles are kept the same. This assumption enables us to simplify the analytical result and clarify the physical mechanism underlying the signals. Considering the assumptions above and the differences in the two components, we obtain the three-pulse photon echo signal of the binary system as

$$I_{\mathrm{Bi}}^{\mathrm{DN}}(\tau, T) = \int_0^\infty \mathrm{d}t\, |\mathcal{I}^{\mathrm{DN}}(\tau, T, t)|^2 \mathcal{A}_{\mathrm{DN}}(\tau, t) \tag{10}$$

where $\mathcal{A}_{\mathrm{DN}}(\tau, t) = 1 + \cos(\Delta\varepsilon_\alpha\tau - \Delta\varepsilon_\beta t)$ is an additional factor that reflects the asymmetry between the components. Here, we consider a simple system with only two components. For a system with more than two components, the additional factor becomes complicated with all the combinations of differences between components. When these differences between components form a continuous distribution, the properties described below will disappear.

Previous theoretical investigations of the two-color three-pulse photon echo were performed on a single dimer system; thus, the term $\mathcal{A}_{\mathrm{DN}}(\tau, t)$ did not appear. The non-integrated signal intensity $|\mathcal{I}^{\mathrm{DN}}(\tau, T, t)|^2$ of the single dimer system reaches its peak at $t \approx \tau$, which results in the peak shift in the integrated intensity. However, our additional term will modify the above behavior of the photon echo signal. To illustrate the modification, we compare the behavior of the non-integrated signal $|\mathcal{I}^{\mathrm{DN}}(\tau, T, t)|^2$ of the single dimer, the additional factor $\mathcal{A}_{\mathrm{DN}}(\tau, t)$, and the overall signal $|\mathcal{I}^{\mathrm{DN}}(\tau, T, t)|^2\mathcal{A}_{\mathrm{DN}}(\tau, t)$ of the binary system for different sets of parameters $\Delta\varepsilon_\alpha$ and $\Delta\varepsilon_\beta$ in Figure 3 at a population time $T = 0$ fs and with the first coherence time set to $\tau = 10$ fs . In the simulations, we choose different Drude−Lorentian spectral densities for chromophores $A$ and $B$

$$\mathcal{J}_i(\omega) = \frac{2\lambda_i\omega_{\mathrm{c}i}\omega}{\omega_{\mathrm{c}i}^2 + \omega^2} \qquad (i = A, B) \tag{11}$$

with reorganization energies $\lambda_A = 60$ cm$^{-1}$ and $\lambda_B = 80$ cm$^{-1}$ and cutoff frequencies $\omega_{\mathrm{c}A} = \omega_{\mathrm{c}B} = 50$ cm$^{-1}$. To calculate the signal, we choose the inhomogeneous broadenings $\sigma_A = 100$ cm$^{-1}$ and $\sigma_B = 50$ cm$^{-1}$ for chromophores $A$ and $B$, respectively, to account for the static disorder. The temperature is set as $T_e = 180$ K. The mean frequencies of chromophores $A$ and $B$ are adjusted to be $\varepsilon_\alpha^0 \equiv (\varepsilon_\alpha^{\mathrm{L}} + \varepsilon_\alpha^{\mathrm{R}})/2 = 760$ nm and $\varepsilon_\beta^0 \equiv (\varepsilon_\beta^{\mathrm{L}} + \varepsilon_\beta^{\mathrm{R}})/2 = 800$ nm. The mixing angle $\theta$ is determined with the coupling constant $J_0 = 280$ cm$^{-1}$ through $\theta = 1/2\ \arctan[2J_0/((\varepsilon_\alpha^0 - \varepsilon_\beta^0)^2 - 4J_0^2)^{1/2}]$. In the simulations, the excitonic energy levels are determined with formulas $\varepsilon_i^{\mathrm{L}} = \varepsilon_i^0 + \Delta\varepsilon_i/2$ and $\varepsilon_i^{\mathrm{R}} = \varepsilon_i^0 - \Delta\varepsilon_i/2$ $(i = \alpha, \beta)$, and the excitonic energy gap is constant. In Figure 3a, we illustrate the signals with the case $\Delta\varepsilon_\alpha = \Delta\varepsilon_\beta = 0$ as the reference for the further discussion. In other cases, the behavior of the signal depends on the signs of $\Delta\varepsilon_\alpha$ and $\Delta\varepsilon_\beta$.

**Case I** $(\Delta\varepsilon_\alpha\cdot\Delta\varepsilon_\beta > 0)$. In this case, $\Delta\varepsilon_\alpha$ and $\Delta\varepsilon_\beta$ have the same sign. The additional factor $\mathcal{A}_{\mathrm{DN}}(\tau, t)$ reaches its maximum at positive time $t = |\Delta\varepsilon_\alpha/\Delta\varepsilon_\beta|\tau$, similar to that of the rephasing pathway signal $\mathcal{I}^{\mathrm{DN}}(\tau, T, t)$ of the single dimer. In Figure 3b, we show the signal maximum position is shifted to a larger $t$ value (red solid line), compared to that of the single dimer (black dotted line). In this calculation, the energy differences between the chromophores are set as $\Delta\varepsilon_\alpha = 140$ cm$^{-1}$ and $\Delta\varepsilon_\beta = 140$ cm$^{-1}$. The peak of the signal of the single dimer (black dotted line) reaches its peak around $t = 5.5$ fs, while the additional factor (blue dashed line) peaks at $t = 10$ fs. The overall signal (red solid line) of the binary system has its maximum at $t = 6.5$ fs.

**Case II** $(\Delta\varepsilon_\alpha\cdot\Delta\varepsilon_\beta < 0)$. Now, $\Delta\varepsilon_\alpha$ and $\Delta\varepsilon_\beta$ have opposite sign. In this case, $\mathcal{A}_{\mathrm{DN}}(\tau, t)$ peaks at a negative value $t = -|\Delta\varepsilon_\alpha/\Delta\varepsilon_\beta|\tau$, which results in an additional decay in the overall signal. The decay is similar to the free induction decay (FID) of the signal from non-rephasing pathways of a single dimer. Thus, we call this decay a pseudo-FID. Figure 3c presents a typical example for the current case, $\Delta\varepsilon_\alpha = 140$ cm$^{-1}$ and $\Delta\varepsilon_\beta = -80$ cm$^{-1}$. The signal of the binary system is shown by the red solid line, which clearly peaks at a smaller value ($t = 3.5$ fs) than that of the single dimer ($t = 5.5$ fs). To evaluate the long time behavior of the peak shift, we include the non-rephasing pathway, shown in Figure 2e−h, to calculate the signal at $\tau < 0$. In the non-rephasing pathways, the order of the first two interactions is reversed, inducing a different coherence compared to that in the rephasing pathways. In this case, the accumulated phase during the first delay is not canceled by the coherence in the third delay. In the overall signal, we have a different additional factor for the non-rephasing pathways

$$\mathcal{A}'_{\mathrm{DN}}(\tau, t) = 1 + \cos(\Delta\varepsilon_\alpha\tau + \Delta\varepsilon_\beta t) \tag{12}$$


dx.doi.org/10.1021/jp409352z | J. Phys. Chem. B 2013, 117, 16416−16421

In contrast to $\mathcal{A}_{DN}(\tau, t)$, $\mathcal{A}'_{DN}(\tau, t)$ reaches its peak at a positive value $t = |\Delta\varepsilon_\alpha/\Delta\varepsilon_\beta|\tau$, which is similar to the rephasing behavior and hereafter called pseudo-rephasing. This pseudo-rephasing mechanism produces a peak in the non-rephasing signal. The combination of pseudo-FID in the rephasing pathways and pseudo-rephasing in the non-rephasing pathways together results in a negative peak shift in the downhill signal.

In Figure 4, we show the linear absorption spectra (Figure 4a) and the peak shift values by the red solid line (Figure 4b) in the downhill measurements as a function of population time $T$ for the different sets of parameters: (1) $\Delta\varepsilon_\alpha = \Delta\varepsilon_\beta = 0$; (2) $\Delta\varepsilon_\alpha = 140\ \text{cm}^{-1}$ and $\Delta\varepsilon_\beta = 140\ \text{cm}^{-1}$ (dashed line); (3) $\Delta\varepsilon_\alpha = 140\ \text{cm}^{-1}$ and $\Delta\varepsilon_\beta = -80\ \text{cm}^{-1}$. In Figure 4b, the increase of peak shift is clearly demonstrated as the solid red line with parameter set 2, in comparison with that with set 1, while the overall decrease of peak shift is observed for set 3. After 200 fs, the peak shift for set 3 becomes negative due to the above mechanisms. However, the small differences in the linear absorption spectra in Figure 4a make it very difficult to distinguish the two parameter sets by means of the spectra. The origin of this ambiguity lies in the similar amplitudes of the inhomogeneous and homogeneous broadening. However, the two-color three-pulse photon echo peak shift measurement is sensitive to the underlying asymmetry.

Let us consider the effect on the signal in the uphill experiment. Here, instead of the first two pulses being at higher frequency, we apply two lower frequency pulses to access the low-lying exciton level $|\beta\rangle$ and probe the system's response at the higher frequency (level $|\alpha\rangle$). The corresponding diagram can be obtained by switching the indices $\alpha$ and $\beta$ in Figure 2. Similarly to the downhill experiment, the signal is explicitly expressed as

$$I_{Bi}^{UP}(\tau, T) = \int_0^\infty dt\, |\mathcal{I}^{UP}(\tau, T, t)|^2 \mathcal{A}_{UP}(\tau, t) \tag{13}$$

where $\mathcal{I}^{UP}(\tau, T, t)$ is the uphill non-integrated signal intensity of the single dimer and $\mathcal{A}_{UP}(\tau, t) = \mathcal{A}_{DN}(t, \tau)$ is the additional factor in uphill experiments. The non-integrated signal can be obtained by switching the indices $\alpha$ and $\beta$ as

$$\mathcal{I}^{UP}(\tau, T, t) = \mathcal{I}^{DN}(\tau, T, t)_{(\alpha\leftrightarrow\beta)} \tag{14}$$

The behavior of the additional factor $\mathcal{A}_{UP}(\tau, t)$ is similar to that in the downhill measurement discussed above. The similar mechanisms result in almost identical features in the uphill signal behavior. We plot the peak shift in the uphill case as a function of population time $T$ (blue dashed lines) in Figure 4b. In the figure, the peak shift value increases when $\Delta\varepsilon_\alpha$ and $\Delta\varepsilon_\beta$ have the same sign ($\Delta\varepsilon_\alpha = 140\ \text{cm}^{-1}$, $\Delta\varepsilon_\beta = 140\ \text{cm}^{-1}$), while it decreases when $\Delta\varepsilon_\alpha$ and $\Delta\varepsilon_\beta$ have the opposite sign ($\Delta\varepsilon_\alpha = 140\ \text{cm}^{-1}$, $\Delta\varepsilon_\beta = -80\ \text{cm}^{-1}$). We also notice a negative peak shift after 200 fs for case II. In the two-color photon echo measurement, the peak shift increases as the coupling $J_0$ becomes stronger.[8] However, the additional factor reduces the peak shift due to the pseudo-FID mechanism in the rephasing pathways for case II. The pseudo-rephasing mechanism appears in the non-rephasing pathway and results in a negative peak shift as $|\Delta\varepsilon_\alpha|$ and $|\Delta\varepsilon_\beta|$ increase in case II. In the current study, we choose a moderately strong coupling strength $J_0 = 280\ \text{cm}^{-1}$, similar to that in the bacterial reaction center.[13] The smaller values of $|\Delta\varepsilon_\alpha|$ and $|\Delta\varepsilon_\beta|$ are required for a negative peak shift, when the coupling $J_0$ of the dimer is weaker.

In the above discussion, the negative peak shift is induced by the asymmetry between the two components of the binary system. A similar asymmetry to that in case II has been observed in the wild-type bacterial reaction center, where each branch has three chromophores, denoted as BChl, BPhy, and P (special pair). The exciton energy differences[19] for the BChl's and BPhy's on the two branches are $\Delta\varepsilon_{BChl} \simeq 150\ \text{cm}^{-1}$ and $\Delta\varepsilon_{BPhy} \simeq -120\ \text{cm}^{-1}$. A previous study[13] suggested that energy transfer to a special pair also results in a negative peak shift. The two mechanisms should be distinguished via experiments on the P-less mutant,[28] in which the special pair has been removed.

The asymmetry also affects the one-color three-pulse peak shift signal, which can be derived by changing $\beta$ to $\alpha$ in the corresponding diagrams. The resultant additional factor reads $\mathcal{A}^{1c} = 1 + \cos[\Delta\varepsilon_\alpha(\tau - t)]$, which is essentially a pseudo-rephasing effect and increases the peak-shift value. The two-color peak shift measurement was shown to enable estimates of the magnitude of the electronic coupling[8,10,12,13] between the chromophores in a single dimer by combining the two-color data with the corresponding value from a one-color experiment. However, the decrease of the peak shift value from two-color measurement on the binary system in case II ($\Delta\varepsilon_\alpha \cdot \Delta\varepsilon_\beta < 0$) leads to an underestimation of the coupling strength, which is characterized by a coefficient $C_{\mu\nu} \equiv 2\sin^2\theta\cos^2\theta$. In the simulation, the coupling coefficient is estimated with the method[10] described by Mančal and Fleming. In Figure 4c, we illustrate the estimated coupling coefficient for three different parameter sets. The gray line shows the exact value $C_{\mu\nu} = 0.362$. The estimated value is smaller in the case ($\Delta\varepsilon_\alpha \cdot \Delta\varepsilon_\beta < 0$) than that of a single dimer ($\Delta\varepsilon_\alpha$, $\Delta\varepsilon_\beta$) = (0, 0). In terms of the coupling strength, the values are underestimated as $J \simeq 275$, 254, and 143 $\text{cm}^{-1}$ for the cases ($\Delta\varepsilon_\alpha$, $\Delta\varepsilon_\beta$) = (20 $\text{cm}^{-1}$, −20 $\text{cm}^{-1}$), (40 $\text{cm}^{-1}$, −40 $\text{cm}^{-1}$), and (80 $\text{cm}^{-1}$, −80 $\text{cm}^{-1}$) respectively, compared to the exact value $J = 280\ \text{cm}^{-1}$.

## 4. CONCLUSIONS

We investigated the two-color photon echo peak shift of a binary system (a pair of dimers) and showed the appearance of an additional factor in the signal. On the basis of this observation, we propose a mechanism involving pseudo-rephasing and pseudo-FID to explain the negative peak shift in the binary system, where the energy differences for two pairs of chromophores have the opposite sign. We also demonstrated an underestimate of the electronic coupling strength via two- and one-color peak shift experiments in such a case.

## AUTHOR INFORMATION

### Corresponding Author

*E-mail: grfleming@lbl.gov.

### Notes

The authors declare no competing financial interest.

## ACKNOWLEDGMENTS

This work was supported by the Director, Office of Science, Office of Basic Energy Sciences, of the USA Department of Energy under contract DE-AC02-05CH11231, the Division of Chemical Sciences, Geo-sciences and Biosciences Division, Office of Basic Energy Sciences through grant DE-AC03-76SF000098 (at LBNL and UC Berkeley), NSF under Contract No. NSF CHE-1012168, and DARPA under grant number N66001-09-1-2026.

## REFERENCES


(1) Mukamel, S. *Principles of Nonlinear Optical Spectroscopy*; Oxford University Press: New York, 1995.

(2) Cho, M. *Two-Dimensional Optical Spectroscopy*; CRC Press: Boca Raton, FL, 2009.

(3) Joo, T.; Jia, Y.; Yu, J.-Y.; Lang, M. J.; Fleming, G. R. Third-order Nonlinear Time Domain Probes of Solvation Dynamics. *J. Chem. Phys.* **1996**, *104*, 6089−6108.

(4) Cho, M.; Yu, J.-Y.; Joo, T.; Nagasawa, Y.; Passino, S. A.; Fleming, G. R. The Integrated Photon Echo and Solvation Dynamics. *J. Phys. Chem.* **1996**, *100*, 11944−11953.

(5) Fleming, G. R.; Cho, M. Chromophore-Solvent Dynamics. *Annu. Rev. Phys. Chem.* **1996**, *47*, 109−134.

(6) Nagasawa, Y.; Yu, J.-Y.; Cho, M.; Fleming, G. R. Excited State Dynamics of Chromophores in Glasses and in Photosynthetic Proteins. *Faraday Discuss.* **1997**, *108*, 23−34.

(7) Groot, M.-L.; Yu, J.-Y.; Agarwal, R.; Norris, J. R.; Fleming, G. R. Three-Pulse Photon Echo Measurements on the Accessory Pigments in the Reaction Center of Rhodobacter Sphaeroides. *J. Phys. Chem. B* **1998**, *102*, 5923−5931.

(8) Yang, M.; Fleming, G. R. Two-color Three-pulse Photon Echoes as A Probe of Electronic Coupling in Molecular Complexes. *J. Chem. Phys.* **1999**, *110*, 2983−2990.

(9) Agarwal, R.; Prall, B. S.; Rizvi, A. H.; Yang, M.; Fleming, G. R. Two-color Three Pulse Photon Echo Peak Shift Spectroscopy. *J. Chem. Phys.* **2002**, *116*, 6243−6252.

(10) Mančal, T.; Fleming, G. R. Probing Electronic Coupling in Excitonically Coupled Heterodimer Complexes By Two-color Three-pulse Photon Echoes. *J. Chem. Phys.* **2004**, *121*, 10556−10565.

(11) Prall, B. S.; Parkinson, D. Y.; Fleming, G. R. Probing Correlated Spectral Motion: Two-color Photon Echo Study of Nile Blue. *J. Chem. Phys.* **2005**, *123*, 054515.

(12) Parkinson, D. Y.; Lee, H.; Fleming, G. R. Measuring Electronic Coupling in the Reaction Center of Purple Photosynthetic Bacteria by Two-Color, Three-Pulse Photon Echo Peak Shift Spectroscopy. *J. Phys. Chem. B* **2007**, *111*, 7449−7456.

(13) Cheng, Y.-C.; Lee, H.; Fleming, G. R. Efficient Simulation of Three-Pulse Photon-Echo Signals with Application to the Determination of Electronic Coupling in A Bacterial Photosynthetic Reaction Center. *J. Phys. Chem. A* **2007**, *111*, 9499−9508.

(14) Allen, J.; Williams, J. Photosynthetic Reaction Centers. *FEBS Lett.* **1998**, *438*, 5−9.

(15) Hoff, A.; Deisenhofer, J. Photophysics of Photosynthesis. Structure and Spectroscopy of Reaction Centers of Purple Bacteria. *Phys. Rep.* **1997**, *287*, 1−247.

(16) Koch, M.; Feldmann, J.; von Plessen, G.; Göbel, E. O.; Thomas, P.; Köhler, K. Quantum Beats versus Polarization Interference: An Experimental Distinction. *Phys. Rev. Lett.* **1992**, *69*, 3631−3634.

(17) Steffen, M. A.; Lao, K.; Boxer, S. G. Dielectric Asymmetry in the Photosynthetic Reaction Center. *Science* **1994**, *264*, 810−816.

(18) King, B. A.; Stanley, R. J.; Boxer, S. G. Excited State Energy Transfer Pathways in Photosynthetic Reaction Centers. 2. Heterodimer Special Pair. *J. Phys. Chem. B* **1997**, *101*, 3644−3648.

(19) Jordanides, X. J.; Scholes, G. D.; Fleming, G. R. The Mechanism of Energy Transfer in the Bacterial Photosynthetic Reaction Center. *J. Phys. Chem. B* **2001**, *105*, 1652−1669.

(20) King, B. A.; de Winter, A.; McAnaney, T. B.; Boxer, S. G. Excited State Energy Transfer Pathways in Photosynthetic Reaction Centers. 4. Asymmetric Energy Transfer in the Heterodimer Mutant. *J. Phys. Chem. B* **2001**, *105*, 1856−1862.

(21) Acharya, K.; Neupane, B.; Zazubovich, V.; Sayre, R. T.; Picorel, R.; Seibert, M.; Jankowiak, R. Site Energies of Active and Inactive Pheophytins in the Reaction Center of Photosystem II from Chlamydomonas reinhardtii. *J. Phys. Chem. B* **2012**, *116*, 3890−3899.

(22) Cho, M.; Fleming, G. R. The Integrated Photon Echo and Solvation Dynamics. II. Peak Shifts and Two-dimensional Photon Echo of A Coupled Chromophore System. *J. Chem. Phys.* **2005**, *123*, 114506.

(23) Tiwari, V.; Peters, W. K.; Jonas, D. M. Electronic Resonance with Anticorrelated Pigment Vibrations Drives Photosynthetic Energy Transfer Outside the Adiabatic Framework. *Proc. Natl. Acad. Sci. U.S.A.* **2013**, *110*, 1203−1208.

(24) Yang, M.; Fleming, G. R. Third-order Nonlinear Optical Response of Energy Transfer Systems. *J. Chem. Phys.* **1999**, *111*, 27−39.

(25) Gelin, M. F.; Egorova, D.; Domcke, W. Efficient Method for the Calculation of Time- and Frequency-resolved Four-wave Mixing Signals and Its Application to Photon-echo Spectroscopy. *J. Chem. Phys.* **2005**, *123*, 164112.

(26) Jonas, D. M. Two-Dimensional Femtosecond Spectroscopy. *Annu. Rev. Phys. Chem.* **2003**, *54*, 425−463.

(27) Schlau-Cohen, G. S.; Ishizaki, A.; Fleming, G. R. Two-dimensional Electronic Spectroscopy and Photosynthesis: Fundamentals and Applications to Photosynthetic Light-harvesting. *Chem. Phys.* **2011**, *386*, 1−22.

(28) Jackson, J. A.; Lin, S.; Taguchi, A. K. W.; Williams, J. C.; Allen, J. P.; Woodbury, N. W. Energy Transfer in Rhodobacter sphaeroides Reaction Centers with the Initial Electron Donor Oxidized or Missing. *J. Phys. Chem. B* **1997**, *101*, 5747−5754.